Journal of *Marine Science and Engineering*

MDPI

Article

Sedimentary Environment Interpretation and Organic Matter Enrichment of the Lower Cambrian Shuijingtuo Shale in the Yichang Slope, South China: Insight from Sedimentary Geochemical Proxies with Major/Trace Elements

Sile Wei [1,*], Mingyi Hu [1], Sheng He [2], Wei Yang [3], Qing He [2], Quansheng Cai [1] and Ping Li [1,*]

[1] School of Earth Sciences, Yangtze University, Wuhan 430100, China; humingyi65@163.com (M.H.); cqsh0713@163.com (Q.C.)
[2] Key Laboratory of Tectonics and Petroleum Resources, Ministry of Education, China University of Geosciences, Wuhan 430074, China; shenghe@cug.edu.cn (S.H.); qinghe@cug.edu.cn (Q.H.)
[3] Guangzhou Marine Geology Survey, China Geological Survey, Ministry of Natural Resources, Guangzhou 510075, China; yangwei@cug.edu.cn
* Correspondence: weisile@outlook.com (S.W.); lip953945568@gmail.com (P.L.)

Abstract: The vertical geochemical variations in total organic carbon (TOC) content and major and trace elements of the Lower Cambrian Shuijingtuo Formation from the Yichang Slope in the Upper Yangtze were investigated to assess the environmental conditions (redox conditions, water mass restriction, terrigenous input, relative sea-level terrestrial, and paleoproductivity) and to determine the primary controlling factors for organic matter enrichment. The Shuijingtuo Shale is divided into three intervals. The lithofacies of interval I are mainly black siliceous shale with high TOC content, and interval II is mainly black siliceous shale with moderate TOC content. Interval III consists of black, clay-rich siliceous shale and dark-gray calcareous shale and is characterized by a low TOC content. The effects of diagenesis and hydrothermal activity on the elements were evaluated prior to analyzing the environmental condition. There are good positive correlations between TOC and U/Al or Mo/Al ratios, suggesting that major/trace elements still retain the geochemical signature of the sedimentary environment. Meanwhile, the geochemical proxies consisting of Al, Fe, Mn, and Ti indicate that the study area did not experience hydrothermal deposits. The redox proxies (U/Th, C_{org}:P_{tot}, and Mo_{EF}–U_{EF}) indicate that the interval I samples were formed under a strong reducing condition. The diagram of TOC vs. Mo indicates that the water mass was moderately restricted during the deposition of interval I shales. Proxies of terrigenous input and relative sea-level (Zr/Al and Zr/Rb) suggest that the organic-rich shales at the bottom were deposited under a relatively high sea-level and experienced minimal input of terrigenous debris from the source area. Additionally, the paleoproductivity indicated by Si_{bio} and (Ni + Cu + Zn)/Al was high for interval I samples. During the interval II period, the relative sea-level began to decline, the seawater still remained in reducing conditions, and there was no change in the productivity, but the input of terrigenous debris increased significantly. In the interval III depositional period, the relative sea-level continued to decrease, the seawater shifted to a dysoxic condition, and the paleoproductivity was also at a lower level. The evolution of the sedimentary environment indicates that the high TOC content in the interval I samples is mainly attributed to the strong reducing condition, the preservation condition and debris dilution together control the organic matter content within the interval II samples, and the low TOC content within the interval III samples is constrained by a combination of the poor preservation conditions and lower paleoproductivity.

Keywords: organic matter enrichment; Shuijingtuo Formation; environmental condition; marine shale

check for updates

Citation: Wei, S.; Hu, M.; He, S.; Yang, W.; He, Q.; Cai, Q.; Li, P. Sedimentary Environment Interpretation and Organic Matter Enrichment of the Lower Cambrian Shuijingtuo Shale in the Yichang Slope, South China: Insight from Sedimentary Geochemical Proxies with Major/Trace Elements. *J. Mar. Sci. Eng.* **2023**, *11*, 2018. https://doi.org/10.3390/jmse11102018

Academic Editor: Antoni Calafat

Received: 31 August 2023
Revised: 8 October 2023
Accepted: 18 October 2023
Published: 20 October 2023

Copyright: © 2023 by the authors. Licensee MDPI, Basel, Switzerland. This article is an open access article distributed under the terms and conditions of the Creative Commons Attribution (CC BY) license (https://creativecommons.org/licenses/by/4.0/).

1. Introduction

Shale gas, as an important unconventional gas reservoirs with extensive resources, has gained increasing attention in countries such as North America and China [1–3]. Gas in shale reservoirs originates from the thermal cracking of petroleum retained during the thermal evolution of organic matter, which leads to the simultaneous formation of numerous organic pores that serve as storage space [4–6]. Therefore, the enrichment of organic matter is closely related to hydrocarbon potential and reservoir quality, which is of great significance in evaluating the exploration potential of shale gas.

Organic matter enrichment in marine sediments is a complex biogeochemical process influenced by various sedimentary environmental factors, such as primary productivity, redox condition, and detrital input [7–10]. Based on the relative contributions of these influencing factors, previous research proposed three models to explain organic matter enrichment, including the productivity model, the preservation model, and the dilution model [11,12]. The productivity model suggests that the organic matter content primarily depends on primary productivity or the productivity of marine organisms [7,8]. In marine environments, the higher productivity of marine organisms such as algae and microorganisms leads to a higher amount of organic matter formed upon their death. However, this model does not explain all cases, as it neglects the influence of preservation conditions and dilution effects on organic matter enrichment [11]. The preservation model assumes that the redox conditions of the seawater environment play a predominant role in the organic matter enrichment [13,14]. Under oxidizing conditions, organic matter is oxidatively decomposed, whereas under reducing conditions, organic matter is more likely to be preserved [14,15]. Thus, if the seawater environment is reducing, the organic matter content will be higher [16]. This model is more applicable when explaining situations where the seawater environment is reducing, particularly in deep ocean settings [17]. The dilution model suggests that the enrichment of organic matter is related to the balance between organic matter input and detrital dilution rate [7,18]. If the deposition rate of organic matter is lower than the dilution rate of terrigenous debris, organic-poor rocks are formed. This condition commonly occurs in marine environments with high inputs of debris, such as offshore and continental shelf areas [11]. These models emphasize the importance of different factors in organic matter enrichment [7]. However, the relative significance of these factors may vary in a certain sedimentary environment. Therefore, a comprehensive analysis of different environmental factors is necessary to gain a more in-depth understanding of the mechanisms of organic matter enrichment.

The Lower Cambrian Shuijingtuo Shale has become an important layer for shale gas exploration in China in recent years, following the success of the Wufeng–Longmaxi Shale [19–21]. It is mainly distributed in the Yangtze block and characterized by a wide sedimentary range, considerable thickness, and high organic matter content [3,20]. Previous studies on the Lower Cambrian Shale have focused on shale pore structure, shale gas adsorption capacity, and organic–inorganic diagenesis [6,20,22–25]. Among these investigations, the content of organic matter has been recognized as an important influencing factor. However, there has been limited research on the mechanisms of organic matter enrichment. This study takes the Lower Cambrian Shuijingtuo Formation in the Yichang Slope as an example to explore the main controlling factors of organic matter enrichment based on a comprehensive analysis of the sedimentary environment. It has significant implications for the selection of favorable exploration areas and the evaluation of high-quality shale intervals in the Lower Cambrian Shuijingtuo Formation.

2. Geological Settings

The Yichang Slope belt is situated in the upper region of the Yangtze block, which together with the Cathaysia block constitutes the South China Plate [17]. Global paleogeographic reconstructions suggested that during the late Ediacaran and early Cambrian transition period (539–514 Ma), the South China Plate was an isolated craton, located in the mid-latitudes of the northern hemisphere, north of the Gondwana continent and consid-

ered to be effectively connected with the open ocean (Figure 1a) [26]. From northeast to southwest, the water depth gradually increases within the Yangtze block, and three marine sedimentary sequences exist, including platform carbonates, shelf calcareous mudstone, slope, and basin shale deposits (Figure 1b). During the early Cambrian Stage 3 (521 Ma), a global transgression event occurred that resulted in the development of organic-rich black shales on the previously deposited carbonate platform (Figure 1c). Subsequently, as the global sea-level dropped 518 million years ago, the lithology of the upper section of the Shuijingtuo Formation transitioned to gray calcareous shale.

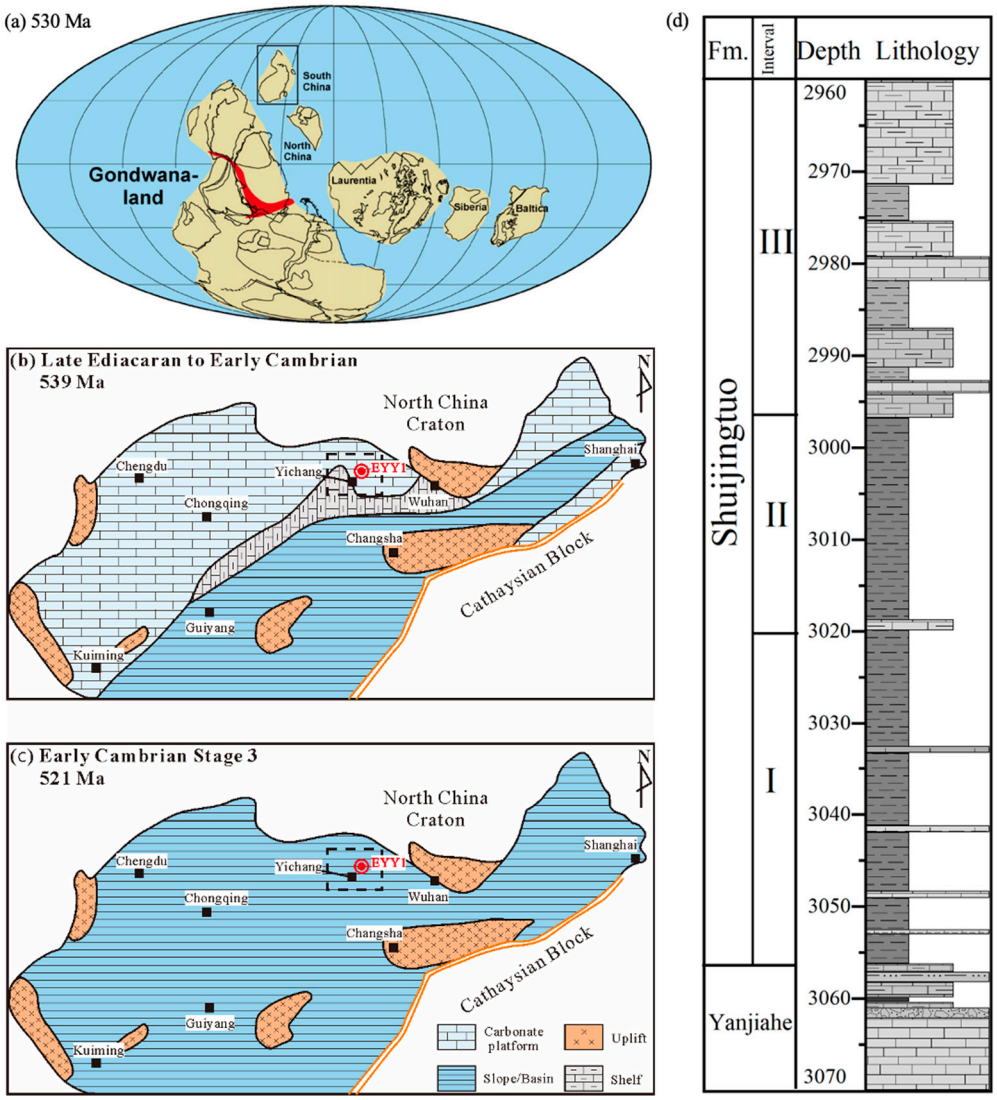

Figure 1. (**a**) Paleogeographic position of the South China Plate during the late Ediacaran and early Cambrian transition period (modified from Li et al. [26]); (**b**) paleogeographic maps of the Yangtze Block at 539 Ma (modified from Jiang et al. [27] and Wang et al. [28]); (**c**) paleogeographic maps of the Yangtze Block in early Cambrian Stage 3 (521 Ma) showing the study area and the location of the investigated well (modified from Jiang et al. [27] and Wang et al. [28]); (**d**) simplified lithologic profile of the Shuijingtuo Formation in the study area.

Based on high-resolution petrology, biostratigraphy, isotope dating, and inorganic geochemistry analysis of South China, the Lower Cambrian Shuijingtuo Formation in the study area can be divided into three intervals (Figure 1d). Interval I consists of black siliceous shale interbedded with thin layers of calcareous mudstone, containing trilobites such as *Tsunyidiscus*, radiolarians, sponge fossils, along with coexisting brachiopods, *Sunella bispinata*, and algae, *Vendotaenia* sp. Interval II comprises black shale that contains abundant

trilobites and brachiopods, as well as brachiopods *Eohadrotreta*, *Palaeobolus*, *Spinobolus*, *Lingulellotreta*, and *Eoobolus*. Interval III is composed of dark-gray calcareous mudstone and carbonaceous limestone.

3. Samples and Methods

A total of 26 Shuijingtuo Formation samples were collected from the EYY1 Well, located in the Yichang Slope, the upper region of the Yangtze block.

3.1. Total Organic Carbon Content

Total organic carbon (TOC) content was conducted using a Rapid CS Cube analyzer. Shale powder samples with particle size less than 75 μm (200 mesh) were placed in silver paper and treated with hydrochloric acid (HCl) at a concentration of 7% by mass to remove the carbonates. The pretreated samples were then dried at 80 °C for 10 h and then subjected to complete combustion using a carrier gas consisting of 99.99% oxygen (O_2) at a temperature of 930 °C. The TOC content was calculated from the amount of carbon dioxide released during the oxidation.

3.2. Thin Section Observation

Thin sections of the Shuijingtuo Shale from the EYY1 Well were observed using transmitted polarized light microscopy (Leica DM4500P) to identify petrographic features including mineral compositions and distributions.

3.3. Major Element Analysis

The analysis of major elements was performed using an X-ray fluorescence spectrometer (XRF) (Zsx Primus II, Rigaku, Japan) at the Wuhan Sample Solution Analytical Technology Co., Ltd., Wuhan, China. The powdered samples were first dried in an oven at 105 °C for 12 h to eliminate free and adsorbed water and then heated to determine the loss on ignition. The X-ray tube utilized was a 4.0 kW end window Rh target, operating at a voltage of 50 kV and a current of 60 mA. All major elemental analysis lines were kα. The data were corrected using the theoretical α coefficient method, and the relative standard deviation was less than 2%. All the samples were processed according to the Chinese National Standard GB/T 14506.28-2010.

3.4. Trace Element Analysis

Trace element analysis was performed by utilizing the Agilent 7700e ICP-MS and at the Wuhan Sample Solution Analytical Technology Co., Ltd., Wuhan, China. The procedure involved drying 200-mesh sample powder at 105 °C for 12 h. Then, 50 mg of the powder was weighed and placed in a Teflon bomb. Slowly, 1 mL each of HNO_3 and HF were added to the bomb. The bomb was placed in a stainless steel pressure jacket and heated at 190 °C for more than 24 h. After cooling, the bomb was opened, and the remaining solution was evaporated on a hotplate at 140 °C. A total of 1 mL of HNO_3 was added and evaporated again. Subsequently, 1 mL each of HNO_3, MQ water, and an internal standard solution of 1 ppm were mixed, sealed, and heated at 190 °C for over 12 h. Finally, the solution was transferred to a polyethylene bottle and diluted to 100 g with 2% HNO_3 for ICP-MS analysis. All the samples were processed according to the Chinese National Standard GB/T 14506.30-2010.

Enrichment factor (EF) is used to reflect the degree of enrichment and depletion of each element and is calculated as follows: element $X_{EF} = (X/Al)_{sample}/(X/Al)_{PAAS}$ [29], where X and Al represent the weight percent concentrations of specified trace elements and aluminum, respectively. Shale samples are normalized using the Post-Archean Australian Shale (PAAS) as a standard reference [30]. $X_{EF} > 1.0$ and $X_{EF} < 1.0$ indicate enrichment and depletion of element X, respectively.

4. Results

4.1. Lithofacies and TOC Content

Based on the core description, thin section observation, and mineral composition, three major lithofacies were identified in the lower area of the Shuijingtuo Formation, including black siliceous shale; black, clay-rich siliceous shale; and dark-gray calcareous shale (Figure 2 and Table 1).

The black siliceous shale is mainly characterized by high silica content (Figure 2a1–a3, b1–b3). The mineral compositions and contents can be referred to in Wei et al. [23]. The black siliceous shale has the highest quartz content and the lowest carbonate mineral content, ranging from 55 to 75 vol.% (average of 62 vol.%) and 4 to 13 vol.% (average of 6 vol.%), respectively. The thin section shows that the black siliceous shale contains an abundance of radiolarians and sponge spicules (Figures 4 and 5 in Wei et al. [23]). The range of TOC content in the black siliceous shale varies widely, with high TOC content (average of 6.02 wt.%) mainly distributed in interval I (Table 1, Figure 2a1–a3) and moderate TOC content (average of 3.94 wt.%) distributed in interval II (Table 1, Figure 2b1–b3).

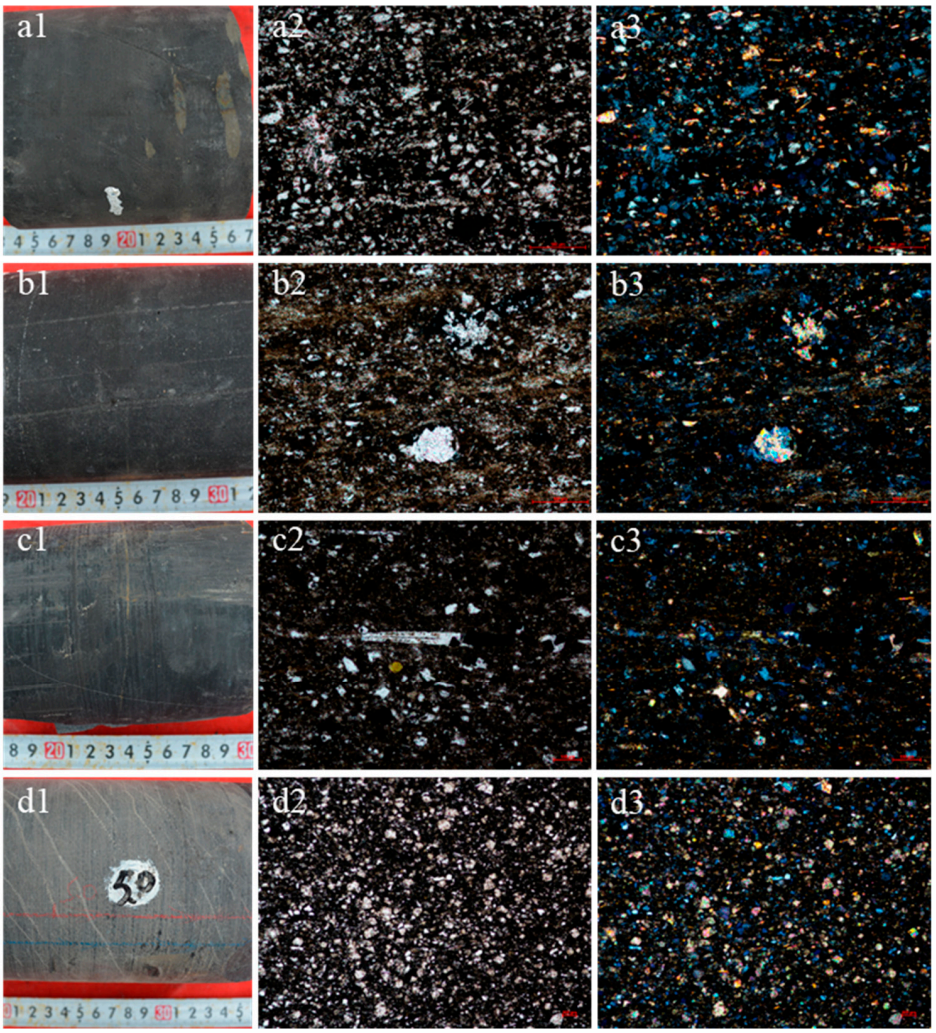

Figure 2. Core and thin section images of the Shuijingtuo Shale. (**a1–d1**) are the core images; (**a2–d2**) are the thin section images observed with the plane-polarized light; (**a3–d3**) are the thin section images observed with cross-polarized light. (**a1–a3**) are the images of the black siliceous shale with high TOC content, 3026.38 m, TOC = 6.20 wt.%; (**b1–b3**) are the images of the black siliceous shale with moderate TOC content, 3007.75 m, TOC = 3.02 wt.%; (**c1–c3**) are the images of the clay-rich siliceous mudstone, 2996.32 m, TOC = 2.27 wt.%; (**d1–d3**) are the images of the dark-gray calcareous mudstone, 2978.08 m, TOC = 1.58 wt.%.

Table 1. Major and trace elements of the Shuijingtuo Shale.

Depth (m)	Interval	TOC (wt.%)	Lithofacies	Al_2O_3 (%)	SiO_2 (%)	CaO (%)	TiO_2 (%)	Fe_2O_3 (%)	MnO (%)	P_2O_5 (%)	Th (ppm)	U (ppm)	Mo (ppm)	Cu (ppm)	Ni (ppm)	Zn (ppm)	Zr (ppm)	Rb (ppm)
2975.53	III	1.63	calcareous S. *	6.21	31.47	25.75	0.28	3.45	0.06	0.08	5.35	3.6	4.2	22.8	26.4	32.0	55.6	56.4
2978.08	III	1.58	calcareous S.	7.73	29.35	22.56	0.36	4.76	0.07	0.11	7.12	4.9	6.2	26.4	33.7	67.2	73.5	69.0
2983.63	III	2.47	clay-rich siliceous S.	12.81	59.62	4.87	0.61	3.32	0.02	0.09	11.4	8.0	16.7	44.0	45.7	48.3	122.0	113.0
2984.98	III	2.21	clay-rich siliceous S.	12.21	60.80	4.98	0.57	3.25	0.02	0.10	12.00	9.4	34.8	60.1	83.2	114	114.0	110.0
2989.32	III	1.80	calcareous S.	7.00	40.68	19.32	0.31	3.90	0.05	0.08	6.10	6.9	14.9	30.7	33.1	37.4	65.0	57.4
2994.23	III	3.27	clay-rich siliceous S.	12.47	55.15	5.61	0.53	4.64	0.04	0.11	10.20	10.3	11.6	58.5	46.4	80.8	107.0	108.0
2996.32	III	2.27	clay-rich siliceous S.	13.02	60.44	2.82	0.55	4.85	0.05	0.10	11.10	7.5	9.18	60.7	44.2	72.6	119.0	112.0
3003.50	II	2.72	siliceous S.	9.49	68.67	3.98	0.41	2.10	0.02	0.08	8.05	15.5	49.1	87.4	107.0	200.0	85.1	80.2
3004.88	II	3.08	siliceous S.	7.21	68.48	5.60	0.29	2.27	0.02	0.11	5.65	21.4	54.0	66.7	113.0	78.8	60.9	56.1
3007.34	II	2.93	siliceous S.	10.71	65.38	2.97	0.42	3.91	0.02	0.13	7.49	21.1	60.2	81.7	119.0	131.0	92.9	88.0
3007.75	II	3.02	siliceous S.	10.42	65.46	3.75	0.42	2.80	0.03	0.14	7.46	18.6	57.8	79.5	106.0	130.0	90.6	83.0
3008.78	II	3.47	siliceous S.	9.45	63.06	5.50	0.38	2.75	0.03	0.18	7.04	23.9	60.5	86.3	116.0	126.0	83.8	75.2
3011.50	II	4.66	siliceous S.	10.11	65.53	3.57	0.45	2.62	0.02	0.11	7.98	31.6	81.4	77.6	118.0	236.0	99.3	82.6
3020.54	I	4.33	siliceous S.	9.20	62.42	5.28	0.50	3.77	0.02	0.18	7.44	47.1	69.9	37.8	127.0	159.0	131.0	70.8
3023.83	I	5.22	siliceous S.	9.40	63.76	4.05	0.52	3.63	0.03	0.17	7.29	44.8	63.2	28.8	151.0	88.6	127.0	69.5
3024.33	I	5.24	siliceous S.	9.27	62.71	4.79	0.51	3.55	0.02	0.15	6.94	47.1	63.6	30.2	142.0	93.0	123.0	67.7
3026.38	I	6.20	siliceous S.	8.84	62.86	5.20	0.48	2.83	0.03	0.16	6.55	57.4	72.2	32.0	148.9	169.0	108.0	64.9
3030.18	I	5.78	siliceous S.	8.68	62.26	4.99	0.47	3.25	0.03	0.15	6.51	33.6	57.4	31.6	145.2	100.0	110.0	61.8
3034.92	I	5.76	siliceous S.	8.09	66.27	3.85	0.43	3.00	0.02	0.12	6.60	65.7	140	38.0	206.0	101.0	98.1	61.1
3037.53	I	4.76	siliceous S.	8.54	57.55	7.26	0.46	3.67	0.03	0.12	6.30	54.2	64.1	31.8	151.9	100.0	100.0	60.6
3041.33	I	5.88	siliceous S.	7.64	64.59	2.89	0.40	5.96	0.02	0.14	5.94	49.2	110	55.1	201.0	105.0	93.0	58.2
3043.48	I	5.08	siliceous S.	7.22	69.82	3.42	0.38	2.44	0.01	0.13	5.60	43.2	81.1	28.8	158.0	54.7	85.8	54.1
3044.76	I	6.06	siliceous S.	5.97	72.98	2.57	0.32	2.21	0.01	0.18	4.68	57.4	102	29.6	185.0	78.3	74.6	44.0
3053.28	I	7.73	siliceous S.	8.13	65.61	2.46	0.44	3.79	0.01	0.13	6.28	43.5	84.6	36.6	136.8	65.4	103.0	68.5
3053.88	I	8.25	siliceous S.	6.58	68.04	3.05	0.36	2.96	0.01	0.10	5.43	42.3	80.9	32.4	153.4	63.0	83.0	53.7
3054.20	I	7.55	siliceous S.	8.57	64.78	2.56	0.46	3.69	0.02	0.15	6.87	56.1	75.2	35.4	173.0	88.1	113.0	69.6

*: The abbreviation "S." stands for shale.

The black, clay-rich siliceous shale presents mainly in interval III of the examined Shuijingtuo Shale and is characterized by moderate to high quartz content (45~48 vol.%, average of 47 vol.%) and moderate clay content (30~34 vol.%, average of 32 vol.%) (Figure 2c1–c3). There is a significant reduction in the radiolarians and sponge spicules in the black, clay-rich siliceous shale compared to the black siliceous shale (Figures 4 and 5 in Wei et al. [23]). The TOC content of the black, clay-rich siliceous shale ranges from 2.21 wt.% to 3.27 wt.% (Table 1).

The dark-gray calcareous shale is also present in interval III. Unlike the other lithofacies, the dark-gray calcareous mudstone has the highest content of carbonate minerals (average of 36 vol.%) and the lowest TOC content (1.67 wt.%) (Figure 2d1–d3). The thin section shows that the siliceous organism is absent in the dark-gray calcareous shale (Figures 4 and 5 in Wei et al. [23]).

Overall, the lithofacies of interval I are mainly composed of black siliceous shale with high TOC content, and interval II is mainly composed of black siliceous shale with moderate TOC content. Interval III consists of black, clay-rich siliceous shale and dark-gray calcareous shale and is characterized by low TOC content.

4.2. Major and Trace Elements

The results of the major and trace elements are listed in Table 1 and the Supplementary Material. The composition of marine shales can be considered to be a mixture of three end-member oxides: SiO_2, Al_2O_3, and CaO, which are closely associated with minerals such as quartz, clay, and carbonates [31]. In general, the Shuijingtuo Shale show varying degrees of enrichment in SiO_2 compared to Al_2O_3 and CaO (Figure 3). The interval I and interval II shale samples have relatively consistent silica concentrations of approximately 64.90 wt.% and 66.10 wt.%, respectively, which are significantly higher than the average of 48.22 wt.% of the interval III samples (Table 1). Conversely, the average CaO content in interval III is 12.78 wt.% (up to 25.75 wt.%), which is much higher than the averages of 4.03 wt.% in interval I and 4.23 wt.% in interval II (Table 1).

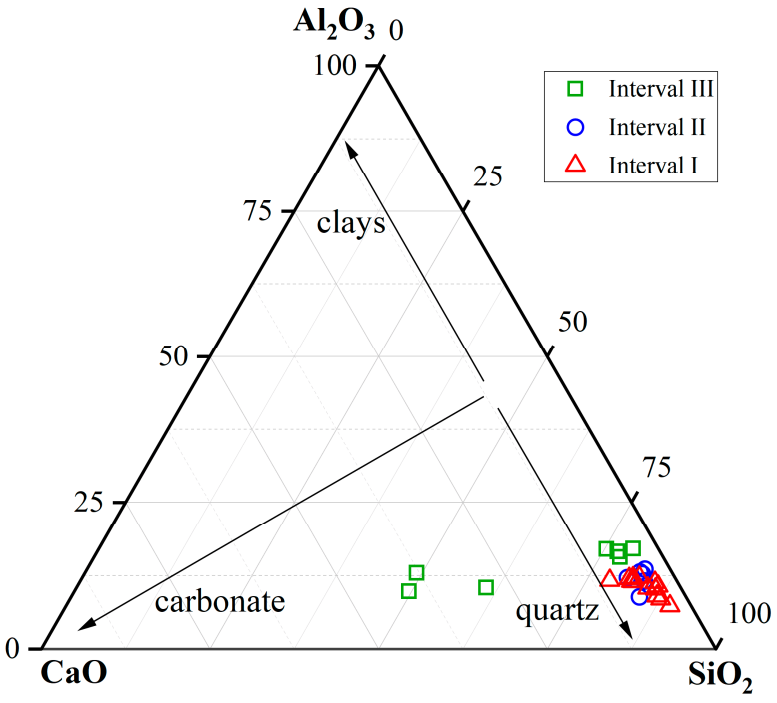

Figure 3. Ternary diagram showing the relative percentages of the major elements SiO_2, Al_2O_3, and CaO.

5. Discussion

5.1. Effect of Thermal Diagenesis and Hydrothermal Activity on Element

5.1.1. Thermal Diagenesis Influence

Organic matter deposited in sediments undergoes maturation due to high temperature and pressure underground, leading to the generation of hydrocarbons, which are then expelled through a rock's pore system. According to Abanda and Hannigan [32], thermal diagenesis and hydrocarbon expulsion can result in a significant loss of trace elements, as organic matter can host up to about 20% of total trace element content. However, Raiswell and Berner [33] argued that although thermal diagenesis does cause a loss of organic matter, and the concentration of trace elements in shale may be lower compared to the original depositional environment, the shale still retains its geochemical signature of deposition. The positive correlation between TOC and U/Al or Mo/Al ratios, proposed by Ross and Bustin [31], can be utilized to assess the impact of thermal diagenesis on the reactivation of elements.

The thermal maturity of the investigated Shuijingtuo Shale is approximately in the dry gas window (~1.93~2.20% Ro), which means that the Shuijingtuo Shale has generated and expelled a certain amount of liquid hydrocarbon [6]. The relationships between TOC content and U/Al as well as Mo/Al ratios are illustrated in Figure 4. It shows a strong positive correlation between both U/Al and Mo/Al ratios and TOC content, suggesting minimal remobilization of elements. Therefore, despite the high thermal maturity of the Shuijingtuo Shale, there is no obvious evidence of element partitioning or remobilization occurring within the examined shale, implying that the elements can be used to reconstruct the paleoenvironmental conditions.

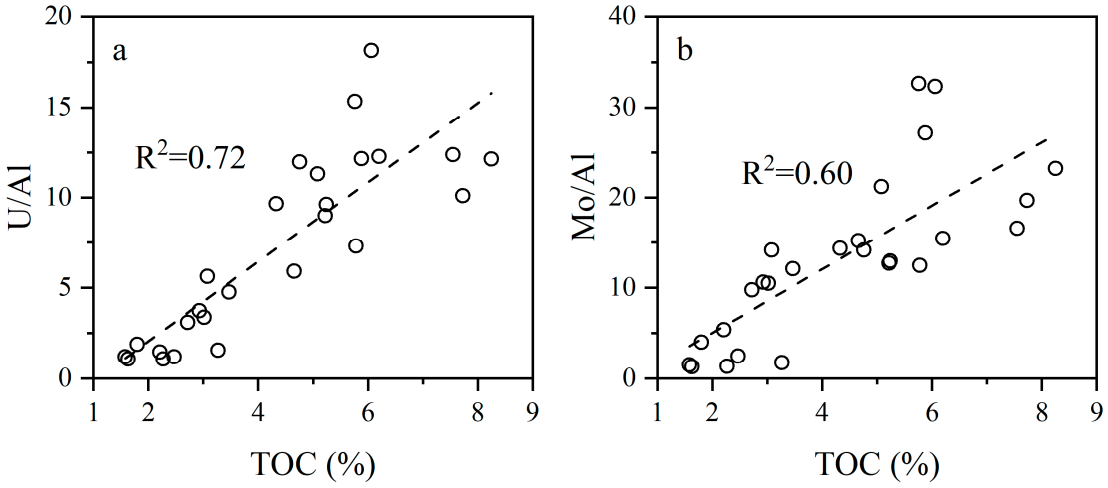

Figure 4. Relationships between TOC content and U/Al (**a**) as well as Mo/Al (**b**).

5.1.2. Hydrothermal Activity Influence

During the early Cambrian, the southern end of the Yangtze block experienced a period of intense rift tectonic activity, resulting in extensive hydrothermal deposition. The combination of major and trace elements, rare-earth elements (REEs), and sulfur isotopes, along with petrological and geological investigations, collectively provide compelling evidence of hydrothermal venting occurrences during this period [34]. Previous studies have revealed the presence of submarine hydrothermal deposits within the Lower Cambrian shale, spanning the southwestern Guizhou Province, the Xiuwu basin within Jiangxi Province, and the western Hunan Province [35,36]. The hydrothermal activity, enriched with volatile components, can alter the chemical conditions of seawater, which would lead to the enrichment and migration of trace elements [37,38]. Therefore, it is necessary to investigate whether the study area has been influenced by hydrothermal activity.

The Al/(Al + Fe + Mn) ratio, Al–Fe–Mn ternary diagram, and Fe/Ti versus Al/(Al + Fe + Mn) plot are widely used to discriminate hydrothermal from non-hydrothermal deposits [23,39–43]. Hydrothermal rocks are typically characterized by Fe- and Mn-rich and Al- and Ti-poor compositions compared to non-hydrothermal rocks [44]. The Al/(Al + Fe + Mn) ratios of the purely hydrothermal rocks are low (<0.01), whereas those of the purely biogenic rocks are greater than 0.60 [39]. The average Al/(Al + Fe + Mn) ratio is 0.66 within the Shuijingtuo Shale, indicating the absence of hydrothermal activity in the study area. The Al–Fe–Mn ternary diagram shows that all analyzed samples fall within the non-hydrothermal zone, characterized by the enrichment of Al relative to Fe and Mn (Figure 5). Furthermore, the Fe/Ti versus Al/(Al + Fe + Mn) plot shows that the data points of the Shuijingtuo Formation are far from the hydrothermal endmember and are situated between the biological and terrigenous endmembers (Figure 6). Therefore, based on the combination of various geochemical indicators, it can be concluded that the study area did not experience hydrothermal activity, which also agrees with the research of Zhang et al. [45], Luo et al. [46], and Wei et al. [47].

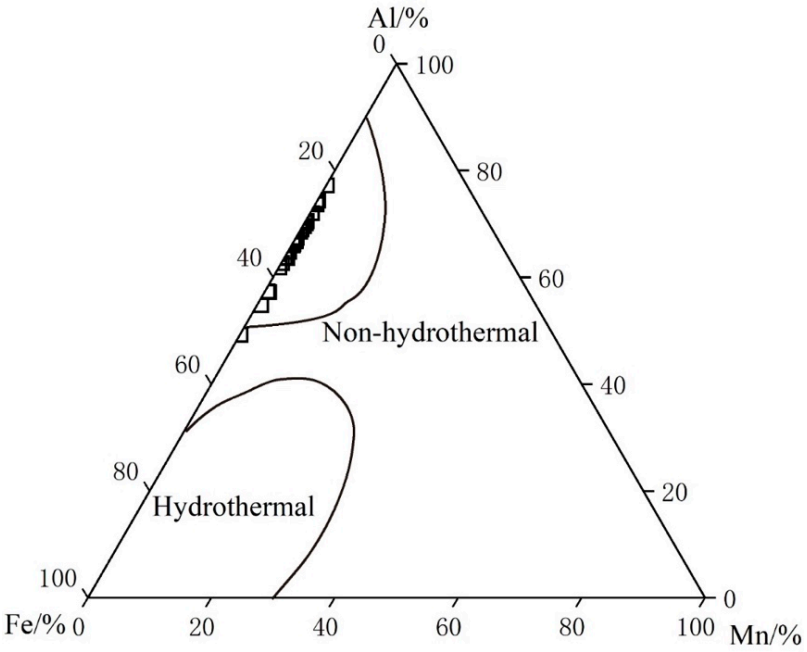

Figure 5. Al–Fe–Mn ternary diagram distinguishing between hydrothermal and non-hydrothermal deposits (modified from Boström and Peterson [39] and Yamamoto [40]).

5.2. Sedimentary Environments

5.2.1. Redox Condition

The ratio of uranium to thorium (U/Th) is a sensitive redox proxy that is most commonly used to interpret the redox conditions of ancient depositional environments [48–50]. Th is relatively immobile in low-temperature surface environments and is typically found in the detrital fraction associated with heavy minerals or clays in shale, where some U is also found [48]. U exists primarily in the hexavalent (6+) and tetravalent (4+) states. Most 6 + U is dissolved and lost during weathering processes, while 4 + U is insoluble and can be fixed under reducing conditions [48,51]. As the process of fixation continues, U is additionally supplied through diffusion in seawater, leading to an increase in the total U/Th ratio. Jones and Manning [48] suggested that a U/Th ratio of >1.25 corresponds to a suboxic and anoxic environment, ~0.75–1.25 corresponds to a dysoxic environment, and <0.75 corresponds to an oxic environment.

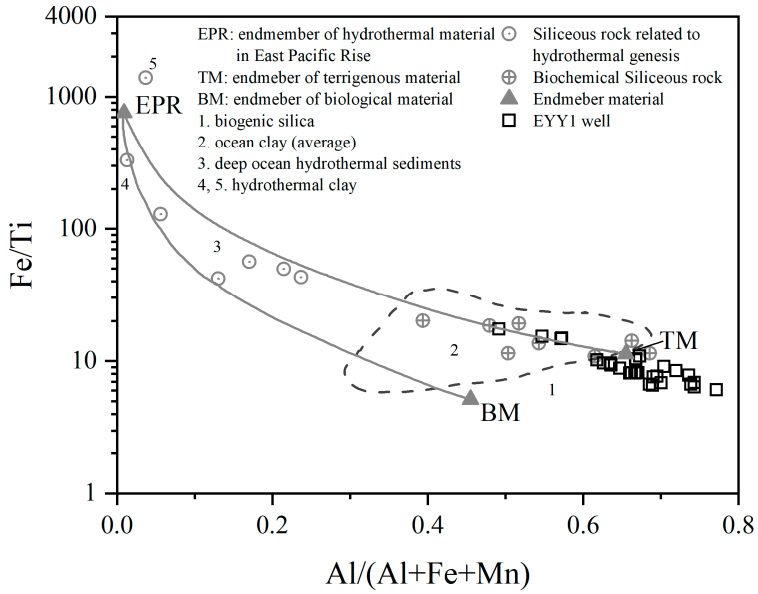

Figure 6. Fe/Ti versus Al/(Al + Fe + Mn) diagram distinguishing between hydrothermal and non-hydrothermal deposits.

The ratio of organic carbon (C_{org}) to organic phosphorus (P_{org}) (C_{org}:P_{org}) in marine sediments is another effective geochemical proxy to assess the redox conditions [14,52]. Most of the P is delivered to the sediment bound in organic matter. The preservation of organic matter and cycle of marine P are closely related to the oxygen level in the water column [52]. In an oxygen-depleted depositional environment, organic matter undergoes degradation, during which P_{org} is released and diffuses into seawater [53]. On the contrary, under oxic conditions, a large amount of P_{org} is captured and bound to sediment through trapping mechanisms such as adsorption, complexation reactions, and biological sequestration [54]. Hence, a higher C_{org}:P_{org} ratio represents a lower oxygen level. Generally, P_{org} is substituted with total P (P_{tot}), as P_{org} accounts for less than 20% of P_{tot} in marine sediments [52]. A C_{org}:P_{tot} ratio > 100 is considered to indicate an anoxic condition, ~50–100 is considered to indicate a dysoxic condition, and <50 is considered to indicate an oxic condition [52].

Figure 7 illustrates the profiles of U/Th and C_{org}:P_{tot} ratios. Both the U/Th and C_{org}:P_{tot} ratios within the interval I shale samples exhibit a considerably wide range, from 5.16 to 12.26 with an average of 7.91 and from 118 to 406 with an average of 216, respectively. These ratios suggest that the depositional environment during interval I was strongly anoxic (Figure 8). The U/Th and C_{org}:P_{tot} ratios within the interval II shale samples vary from 1.93 to 3.96 with an average of 3.07 and from 94 to 203 with an average of 139, respectively (Figure 7). Although the values of U/Th and C_{org}:P_{tot} ratios in the interval II shale samples are lower than those in interval I, they still exceed the critical values of the anoxic condition. Therefore, interval II was also deposited under an anoxic condition, albeit with a weaker reducing intensity. In contrast, the U/Th and C_{org}:P_{tot} ratios of the interval III shale samples demonstrate a relatively low value, ranging from 0.67 to 1.13 and from 73 to 155, respectively (Figure 8). These values suggest a dysoxic depositional environment, characterized by low to moderate levels of oxygen.

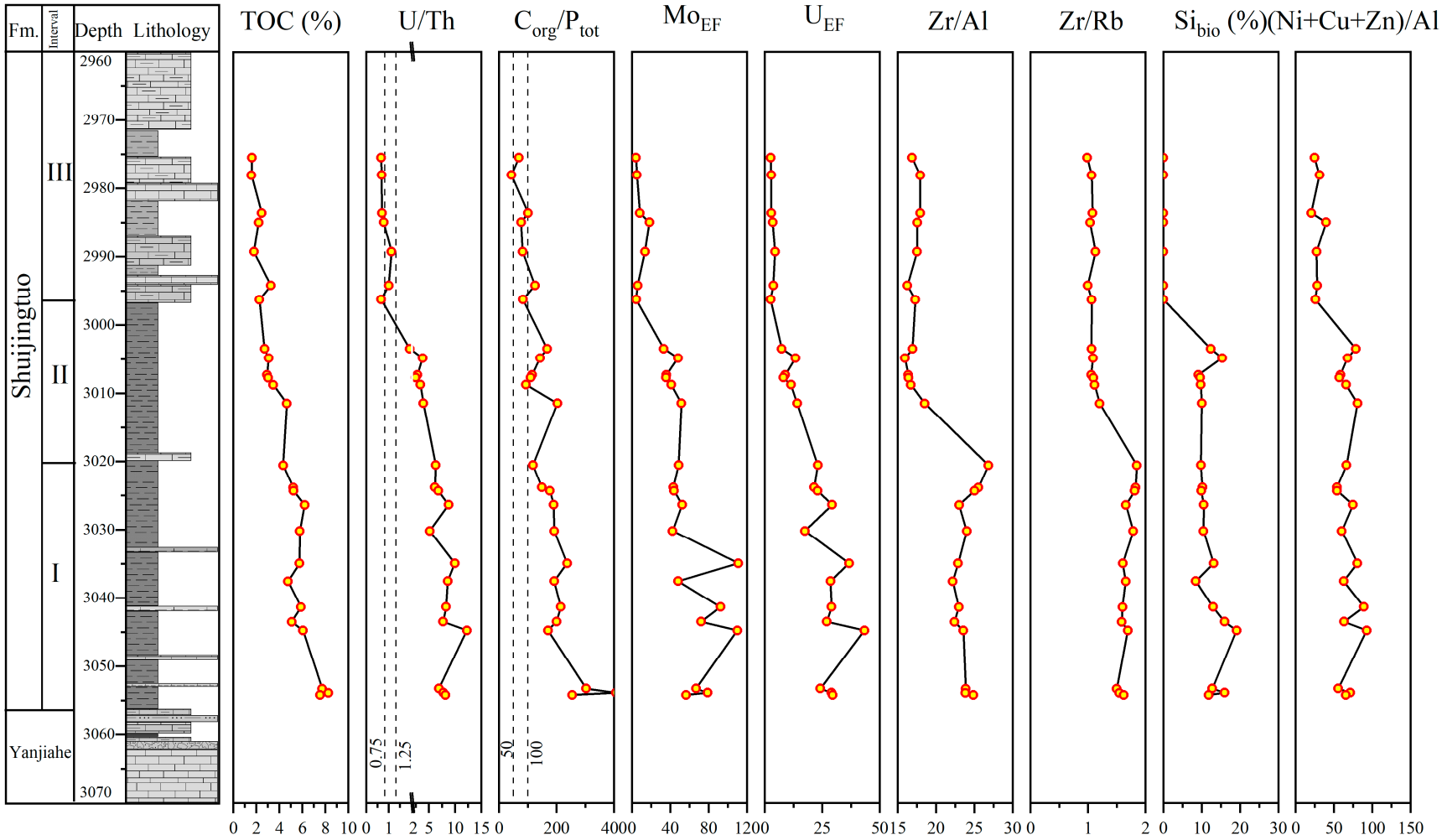

Figure 7. Stratigraphic profiles of redox conditions proxies (U/Th, C_{org}:P_{tot}), water mass restriction proxies (Mo_{EF}, U_{EF}), terrigenous input and relative sea-level proxies (Zr/Al, Zr/Rb), and paleoproductivity proxies (Si_{bio}, (Ni + Cu +Zn)/Al) of the EYY1 well.

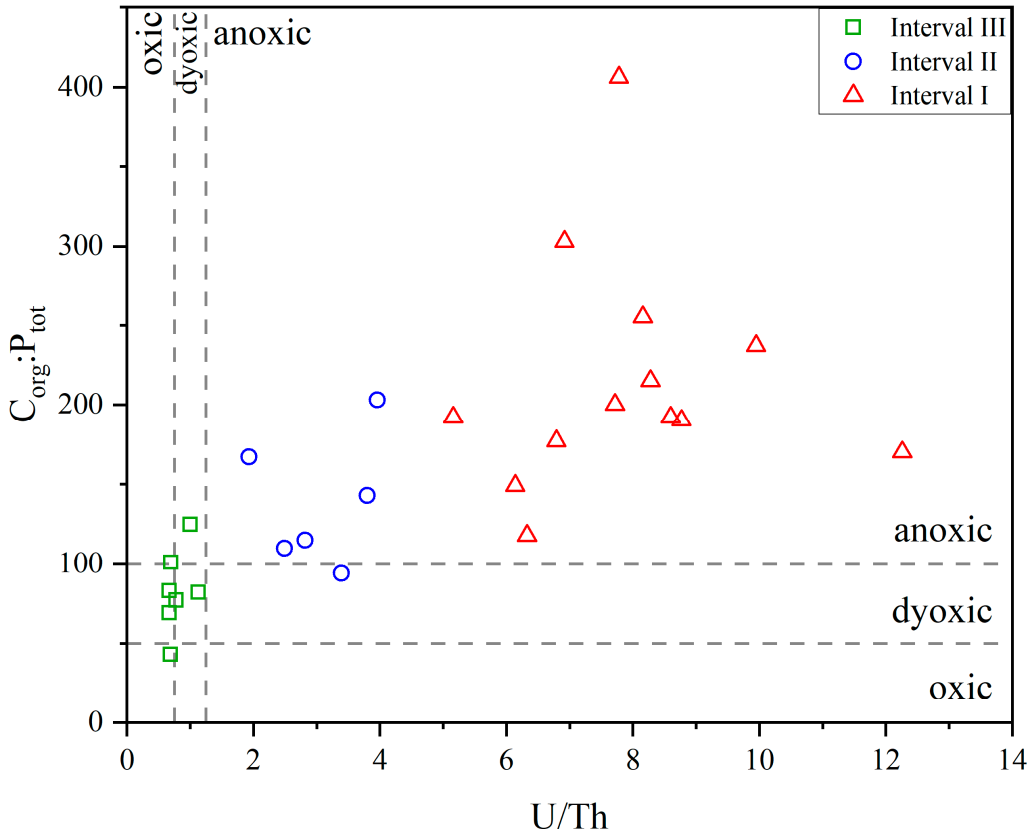

Figure 8. Cross plot of the U/Th and C_{org}:P_{tot} ratio reflecting the redox conditions of the Shuijingtuo Shale.

The variations in redox conditions in the EYY1 Well of this study exhibit comparability with another well in the study area, the EYY3 Well [17]. These two wells demonstrate similar changes in redox intensity vertically, with both showing an anoxic condition at the bottom [17]. However, the difference lies in the middle and upper parts, where dysoxic and oxic conditions are observed in the EYY3 Well, respectively, with a significantly lower reducing intensity compared to the EYY1 Well in this study [17]. This difference is probably attributed to the fact that the EYY3 Well is located in the platform depression zone of the Yichang Slope, where the water depth is shallower compared to the EYY1 Well, which is located in the continental shelf [23,55].

5.2.2. Water Mass Restriction

Patterns of molybdenum–uranium (Mo_{EF}–U_{EF}) covariation are extensively utilized to assess the water mass restriction and redox conditions, primarily because of their low concentrations in the upper continental crust, near-uniform concentrations in seawater worldwide, and predominantly authigenic uptake and enrichment from seawater [28,56–58]. The similarity in Mo–U relationships between modern marine systems and paleomarine systems allows the former to be used to explain paleoenvironmental parameters.

The examined Shuijingtuo Shale demonstrates a significant level of enrichment in Mo and U compared to the PAAS background sample (Figures 7 and 9). It shows that the Mo_{EF} is more enriched than the U_{EF}, which was also reported in the Wufeng–Longmaxi Shale in the Sichuan Basin [14,59,60]. A possible explanation for the low U_{EF} is that some U may have been lost during the hydrocarbon expulsion process, despite the fact that U is not typically the most abundant trace metal in kerogen [57]. Samples from interval III exhibit U_{EF} values that are close to 3, while the Mo_{EF} varies considerably, with a maximum value

of up to 18 (average of 8.62, standard deviation 5.36). When the U_{EF} is higher than 3, the Mo_{EF} and the U_{EF} tend to increase equally on a logarithmic scale in interval I and interval II (Figure 9). With the exception of a few samples, the majority of the Shuijingtuo samples follow the unrestricted marine trend (Figure 9). The interval II samples conform almost completely to the trend, whereas the interval I samples scatter around the unrestricted marine trend (Figure 9). Therefore, there is some variation in the fidelity of ancient ocean systems in following the present-day unrestricted marine trend.

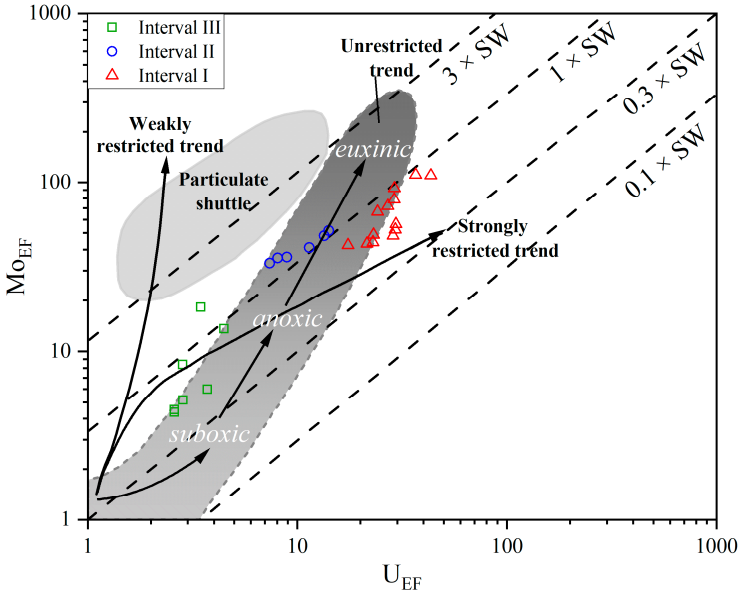

Figure 9. Mo_{EF}–U_{EF} covariation in the Shuijingtuo Shale (modified from Tribovillard et al. [57]).

The paleoredox interpretations based on the Mo_{EF}–U_{EF} covariation are in excellent agreement with those based on the geochemical proxies U/Th and C_{org}:P_{tot} ratios (Figure 9).

The diagram of TOC vs. Mo can be used to evaluate the degree of water mass restriction that cannot be accounted for by the Mo_{EF}–U_{EF} covariation [57,58,61]. Among the analyzed Shuijingtuo samples, interval I samples have the highest TOC and Mo content (Figure 10), as the organic matter can promote Mo adsorption by the sediment under highly anoxic conditions [57]. The Mo/TOC ratio of the interval I shales (ranging from 10 to 24, average of 14) falls between the Framvaren Fjord (Mo/TOC = 9) and the Cariaco Basin (Mo/TOC = 25) (Figure 10), suggesting that the water mass was moderately restricted during the deposition of interval I shales. Interval II samples are mainly located on the left of the Saanich Inlet trend line (Figure 10), indicating a low degree of water mass restriction. The TOC–Mo plot makes it difficult to assess the degree of mass restriction of interval III because the data points cross multiple lines of different degrees of restriction (Figure 10). However, based on the redox conditions and the lower Mo and TOC values, it is reasonable to infer that the water mass restriction of interval III is weak.

5.2.3. Terrigenous Input and Relative Sea-Level

Despite the relative stability of the marine sedimentary environment, continental shelves and slopes close to the source area experience an influx of terrigenous debris that can alter the depositional rate, rock composition, and abundance of organic matter [18,62]. Detrital-derived elements, such as aluminum (Al), zirconium (Zr), and rubidium (Rb), are commonly used as proxies for the sediment transport distance and transport energy [29,63]. Al is found in the aluminosilicate fraction of sediments, predominantly in clay minerals, which have the capacity to be transported over long distances. Similar to Al, Rb is a light element that exists in K-feldspar, mica, and clay minerals and is also capable of long-distance transport [63,64]. Conversely, Zr is mainly associated with heavy minerals such

as zircon ($ZrSiO_4$), which has a limited transport distance [63]. Therefore, trends in Zr (expressed as Zr/Al and Zr/Rb ratios) can reflect the changes in terrigenous input and relative sea-level.

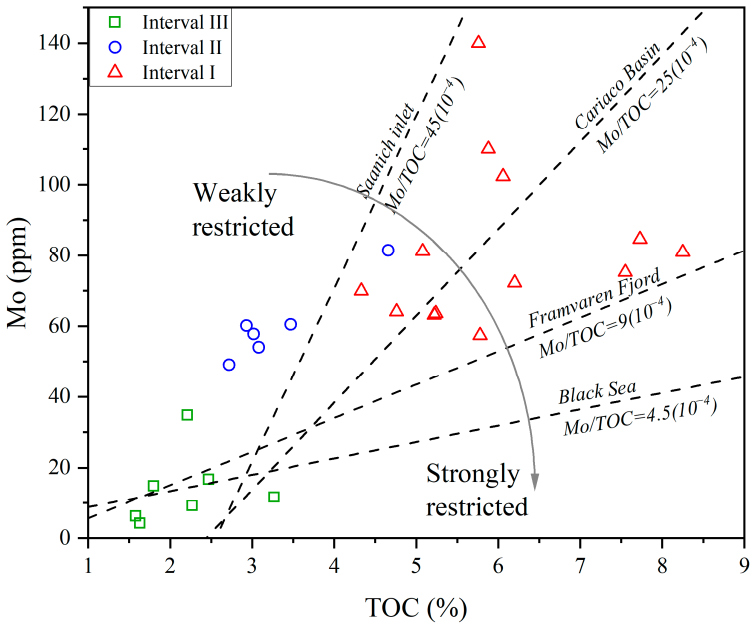

Figure 10. Cross plot of TOC content versus Mo showing the water mass restriction of the Shuijingtuo Shale (modified from Tribovillard et al. [57]).

The profiles of the Zr/Al and Zr/Rb ratios show similar variations (Figure 7). In the initial interval I period, the Zr/Al ratio ranges from 22.19 to 26.84, with an average of 23.93. After the deposition of interval I, the Zr/Al ratio within the interval II and interval III samples of the EYY1 Well sharply decrease and remain relatively stable, ranging from 15.97 to 18.54 (average of 17.09). The Zr/Al ratios and their variations at the bottom of the EYY1 Well are consistent with the EYY3 Well, both exhibiting relatively high values with a small fluctuation range [17]. Additionally, the lithology of both wells is predominantly composed of siliceous shale. However, in the middle and upper parts, the Zr/Al ratio in the EYY3 Well gradually decreases, which is distinct from the sharp decrease observed in the EYY1 Well. The comparison between the EYY1 and EYY3 Wells illustrates that the decline of relative sea-level has a greater impact on the continental shelf area. In the EYY1 Well, the profile of the Zr/Rb ratio exhibits a similar variation pattern to that of the Zr/Al. In interval I, it shows high values and a small fluctuation range (1.50~1.85, average of 1.67), while in intervals II and III, it rapidly decreases and remains relatively stable (0.99~1.20, average of 1.08).

The trend observed in the Zr/Al and Zr/Rb ratios suggests that the relative sea-level was at its highest and most stable during the interval I depositional period of the EYY1 Well. It experienced minimal input of terrigenous debris from the source area. During the interval II and interval III depositional periods, the study area underwent a sharp decline in relative sea-level, accompanied by a large influx of terrigenous sediments.

5.2.4. Paleoproductivity

Biogenic silica (Si_{bio}) was widely used as a geochemical proxy to assess paleoproductivity [65,66]. The common sources of silica in shales include the dissolution of siliceous skeletons (biogenic silica), transition of smectite to illite (clay-derived silica), pressure dissolution of detrital quartz, alteration of feldspar, alteration of volcanic ash, and precipitation of submarine hydrothermal venting [67–69]. In our previous study, we ruled out hydrothermal origin and suggested that no volcanic ash alteration occurred within the Shuijingtuo Shale in the study area [23]. The silica in the examined shale samples is mainly

biological and of terrestrial depositional origin. The Si_{bio} was calculated as the absolute difference between Si measured in a sample and the Si versus Al regression line (detrital trend line). The detailed method can be found in Wei et al. [23].

Nickel (Ni), copper (Cu), and zinc (Zn) are trace metals that are essential micronutrients for the growth of marine organisms [29]. The sum of Ni, Cu, and Zn serves as a more dependable indicator of paleoproductivity. This is primarily due to its lower susceptibility to postdepositional alterations and diagenesis, as opposed to analyzing each element individually. To eliminate the effects of debris dilution, (Ni + Cu + Zn)/Al is suggested to be used for the qualitative assessment of paleoproductivity.

The Si_{bio} profile shown in Figure 7 has a distinct pattern of variation. The profile shows that Si_{bio} has a maximum at the bottom of interval I, then begins to decrease slightly during the middle and late stage of interval I, continues through the interval II period, and then declines rapidly to a minimum of nearly zero in interval III. Overall, Si_{bio} remains at a high level during the interval I and interval II periods and is almost absent during the interval III period. The variation in (Ni + Cu + Zn)/Al is similar to that in Si_{bio} (Figure 7). As a whole, (Ni + Cu + Zn)/Al ratios maintain high values (average value 68.32) within the interval I and interval II samples, which are significantly higher than those of the interval III samples (average value 28.23). For the same continental shelf sedimentation in the upper Yangtze block, the value of Ni + Cu + Zn in the study area, where there is no hydrothermal activity, is significantly lower than that in areas with hydrothermal activity, reaching a maximum value of 3470 ppm [70]. This is because hydrothermal activity can replenish a large number of trace elements into seawater. The lower values of Ni + Cu + Zn can also indicate, to some extent, the absence of hydrothermal activity in the study area. The trend of Si_{bio} and (Ni + Cu + Zn)/Al reflects changes in paleoproductivity, which experiences a rapid decline from high productivity levels in the interval I and interval II periods to lower levels in the interval III period. These changes in paleoproductivity are also supported by variations in the abundance of siliciclastic biogenesis observed in the thin sections reported by Wei et al. [23].

5.3. Sedimentary Environment of the Shuijingtuo Shale

The rapid rise in relative sea-level was one of the significant global geologic events that occurred during the late Ediacaran to the early Cambrian. Analysis of the TOC–Mo diagram indicates that during the interval I stage, the study area transformed into a moderate restriction sea due to the surrounding paleohighs in the upper Yangtze block (Figure 11). The restricted sea was characterized by strong anoxic conditions, indicated by the redox proxies (U/Th and C_{org}:P_{tot}) observed in the interval I samples (Figure 11). The significant abundance of siliceous organisms, especially the presence of sponge spicules fossils, and the high biogenic silica content in the interval I samples suggest that the connectivity between the upper Yangtze and the open ocean greatly increased the paleoproductivity. Simultaneously, the high relative sea-level reduced the input of terrestrial debris, as evidenced by the high Zr/Al and Zr/Rb ratios (Figure 11).

During the interval II stage, the relative sea-level in the study area began to decline, leading to a series of changes in the sedimentary environment. The most noticeable change is that the water mass restriction shifted from a moderately restricted sea to a weakly restricted sea, while the seawater remained under reducing conditions, albeit with lower reduction than in the interval I stage. Additionally, the input of detrital material into the study area increased significantly due to the longer migration distance of terrestrial debris caused by the fall in the relative sea-level.

With the continuous decline of the relative sea-level, the water depths during the interval III period were at their lowest, exhibiting characteristics of a shallow shelf environment. The wide and shallow sedimentary environment has developed a marine stratigraphy characterized by dark-gray calcareous mudstone interbedded with shales. The low values of the U/Th and C_{org}:P_{tot} indicate that during the interval III period, the seawater was under a dysoxic depositional condition. Furthermore, the input of terrigenous debris, indicated

by the Zr/Al and Zr/Rb ratios, was kept at a stable, high level. Additionally, the nutrients (Ni + Cu +Zn)/Al necessary for microbial growth and development were reduced.

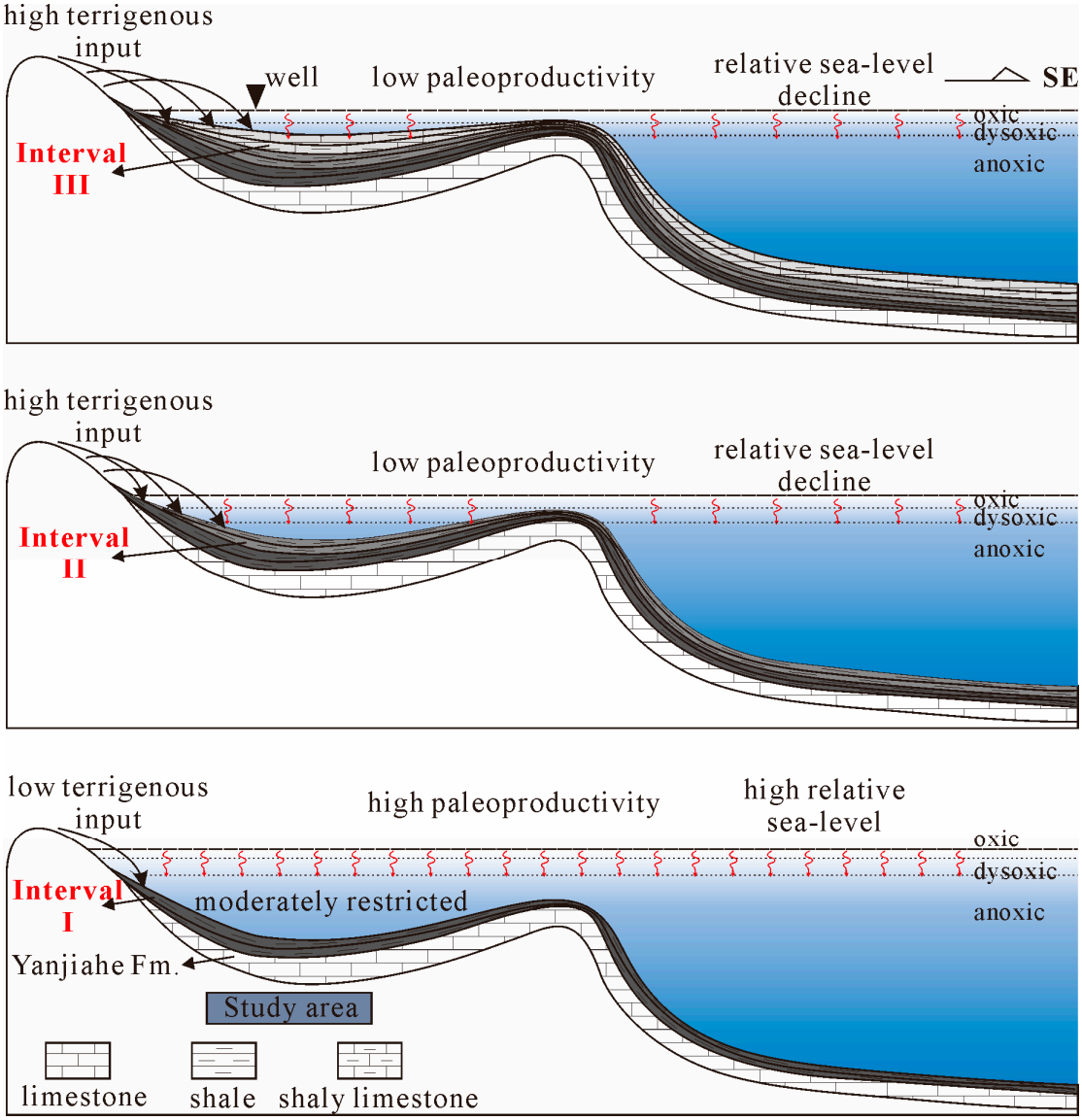

Figure 11. Schematic interpretation of the evolution of the sedimentary environment during the deposition of the Shuijingtuo Shale.

5.4. Main Factors Controlling Organic Matter Enrichment

The predominant factor controlling the high TOC content of the interval I shale samples is the strong reducing condition. The paleoproductivity of the interval I period was high and remained relatively stable, which does not match the decreasing trend of TOC content with decreasing burial depth (Figures 7 and 12e,f). This suggests that although paleoproductivity was high during the interval I period, it was not the primary controlling factor for TOC enrichment. Similarly, the input of terrigenous debris remained low during this depositional period and showed an increasing trend in the late interval I period, which does not agree with the variations in TOC content (Figures 7 and 12c,d). However, there is a strong synergistic trend between the redox proxies and TOC content (Figure 12a,b), indicating that the intense anoxic conditions caused by the deep seawater were conducive to preserving a substantial amount of organic matter. Therefore, through the comprehensive analysis, it can be concluded that the high TOC contents in the shale at the bottom of the

Shuijingtuo Formation during the interval I depositional period were primarily controlled by the strongly reducing depositional environment.

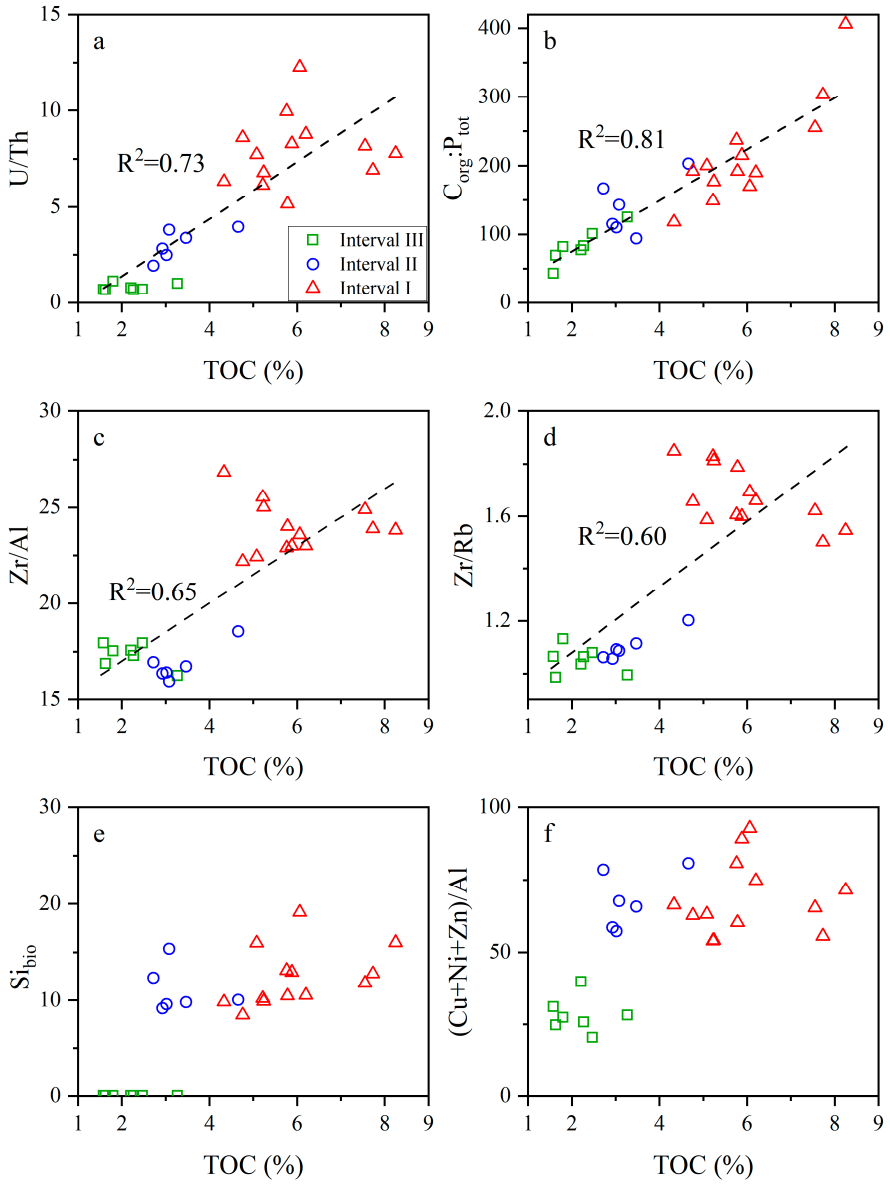

Figure 12. Relationships between the TOC content and the sedimentary geochemical proxies.

The variations in TOC content during the interval II period were controlled by favorable preservation conditions and the dilution effect of terrigenous debris. Overall, both the Si_{bio} and (Ni + Cu + Zn)/Al in the interval II samples are approximately equal to or little higher than those of the interval I samples (Figures 7 and 12e,f), indicating that there was no significant change in paleoproductivity. However, the TOC content within the interval II samples is lower than that in the interval I samples, indicating that despite the higher paleoproductivity levels, there was no corresponding increase in TOC content. After the deposition of interval I strata, oxygen concentration decreased due to the decline in the relative sea-level, but the environment still remained in a reducing state during the interval II period. The strong correlations between the TOC content and the redox indicators (Figure 12a,b) suggest that the reducing conditions remain the main controlling factor for the organic matter enrichment. The increased input of terrigenous debris caused by the fall in the relative sea-level diluted the original concentration of organic matter (Figure 12c,d), which is another factor leading to the decrease in TOC content during the interval II pe-

riod. Therefore, the changes in TOC content within the interval II samples are primarily controlled by the reducing environment, followed by the input of terrigenous detritus.

The low TOC content within the interval III samples is constrained by a combination of the poor preservation conditions and the lower paleoproductivity. During the deposition of the interval III, the relative sea-level continued to fall, while the input of terrigenous debris remained relatively stable compared to interval II (Figure 7). It is clear that the dilution effect of terrigenous debris does not adequately account for the upward decrease in TOC content within the interval III samples (Figure 12c,d). The redox geochemical indicators suggest that the interval III samples were deposited under a dysoxic condition, where the preservation conditions for organic matter were relatively poor. This shows that TOC content has a good synergistic variation with the U/Th and C_{org}:P_{tot} within the interval III samples (Figure 12a,b), indicating that samples with relatively high oxygen concentrations, i.e., poor preservation conditions, have lower TOC content. Moreover, paleoproductivity was also at a lower level. There is a weak positive correlation between TOC content and (Cu + Ni + Zn)/Al values (Figure 12e,f). Based on the aforementioned analysis, we conclude that the low TOC content within the interval III samples is primarily associated with poor preservation conditions and lower paleoproductivity levels.

6. Conclusions

1. The Lower Cambrian Shuijingtuo Shale in the Yichang Slope is divided into three intervals. The lithofacies of interval I is mainly black siliceous shale with high TOC content, and interval II is mainly black siliceous shale with moderate TOC content. Interval III consists of black, clay-rich siliceous shale and dark-gray calcareous shale and is characterized by a low TOC content.
2. The major and trace elements in the examined gas-matured samples still retain the geochemical signature of the sedimentary environment, because the thermal diagenesis has little effect on element partitioning or remobilization. This is supported by the strong positive correlations observed between both U/Al and Mo/Al ratios and TOC content. The geochemical indicators used to distinguish between hydrothermal and non-hydrothermal activity reveal that the hydrothermal deposits, which were widely distributed in the southern Yangtze block, were absent in the Yichang Slope.
3. Based on the evolution of the sedimentary environment, the primary controlling factors for the organic matter enrichment in the Shuijingtuo Formation at different stages are determined. The high TOC content in the interval I samples is mainly attributed to the strong reducing condition, which was caused by the rapid rise of the relative sea-level in the late Ediacaran to early Cambrian. The subsequent decline in the relative sea-level after the interval II period led to a decrease in oxygen concentration. Additionally, the input of abundant terrigenous debris diluted the original organic matter concentration. Thus, preservation condition and debris dilution together control the organic matter content within the interval II samples. As the relative sea-level continued to fall, the preservation conditions and primary productivity reached lower levels, resulting in lower TOC content in the interval III samples.

Supplementary Materials: The following supporting information can be downloaded at: https://www.mdpi.com/article/10.3390/jmse11102018/s1, Table S1: results of all the major and trace elements.

Author Contributions: Conceptualization, S.W., M.H., S.H. and P.L.; methodology, S.W., M.H., S.H., W.Y. and P.L.; formal analysis, S.W., Q.H. and Q.C.; investigation, Q.H., W.Y. and Q.C.; resources, M.H. and S.H.; data curation, Q.H., W.Y. and P.L.; writing—original draft preparation, S.W. and P.L.; writing—review and editing, S.W., M.H., S.H., Q.H., W.Y., Q.C. and P.L.; funding acquisition, S.W., S.H. and Q.C. All authors have read and agreed to the published version of the manuscript.

Funding: This research was funded by the Natural Science Foundation of Hubei Province (No. 2022CFB652) and CNPC Innovation Found (No. 2021DQ02-0101).

Institutional Review Board Statement: Not applicable.

Informed Consent Statement: Not applicable.

Data Availability Statement: Data supporting the results can be found in the manuscript text, tables, and figures.

Conflicts of Interest: The authors declare no conflict of interest.

References

1. Curtis, J.B. Fractured shale-gas systems. *AAPG Bull.* **2002**, *86*, 1921–1938.
2. Hao, F.; Zou, H.; Lu, Y. Mechanisms of shale gas storage: Implications for shale gas exploration in China. *AAPG Bull.* **2013**, *97*, 1325–1346. [CrossRef]
3. Zou, C.; Yang, Z.; Dong, D.; Zhao, q.; Chen, Z.; Feng, Y.; Li, J.; Wang, X. Formation, distribution and prospect of unconventional hydrocarbons in source rock strata in China. *Earth Sci.* **2022**, *47*, 1517–1533. (In Chinese)
4. Ko, L.T.; Loucks, R.G.; Zhang, T.; Ruppel, S.C.; Shao, D. Pore and pore network evolution of Upper Cretaceous Boquillas (Eagle Ford-equivalent) mudrocks: Results from gold tube pyrolysis experiments. *AAPG Bull.* **2016**, *100*, 1693–1722. [CrossRef]
5. Loucks, R.G.; Reed, R.M.; Ruppel, S.C.; Jarvie, D.M. Morphology, genesis, and distribution of nanometer-scale pores in siliceous mudstones of the Mississippian Barnett Shale. *J. Sediment. Res.* **2009**, *79*, 848–861. [CrossRef]
6. Wei, S.; He, S.; Pan, Z.; Zhai, G.; Yang, R.; Dong, T.; Yang, W. Characteristics and evolution of pyrobitumen-hosted pores of the overmature Lower Cambrian Shuijingtuo Shale in the south of Huangling anticline, Yichang area, China: Evidence from FE-SEM petrography. *Mar. Petrol. Geol.* **2020**, *116*, 104303. [CrossRef]
7. Sageman, B.B.; Murphy, A.E.; Werne, J.P.; Ver Straeten, C.A.; Hollander, D.J.; Lyons, T.W. A tale of shales: The relative roles of production, decomposition, and dilution in the accumulation of organic-rich strata, Middle–Upper Devonian, Appalachian basin. *Chem. Geol.* **2003**, *195*, 229–273. [CrossRef]
8. Katz, B.J. Controlling Factors on Source Rock Development—A Review of Productivity, Preservation, and Sedimentation Rate. In *The Deposition of Organic-Carbon-Rich Sediments: Models, Mechanisms, and Consequences*; SEPM Society for Sedimentary Geology: Broken Arrow, OK, USA, 2005; Volume 82, pp. 7–16.
9. Zhao, J.; Jin, Z.; Jin, Z.; Geng, Y.; Wen, X.; Yan, C. Applying sedimentary geochemical proxies for paleoenvironment interpretation of organic-rich shale deposition in the Sichuan Basin, China. *Int. J. Coal Geol.* **2016**, *163*, 52–71. [CrossRef]
10. Algeo, T.J.; Maynard, J.B. Trace-element behavior and redox facies in core shales of Upper Pennsylvanian Kansas-type cyclothems. *Chem. Geol.* **2004**, *206*, 289–318. [CrossRef]
11. Harris, N.B. *The Deposition of Organic-Carbon-Rich Sediments: Models, Mechanisms, and Consequences—Introduction*; SEPM Society for Sedimentary Geology: Broken Arrow, OK, USA, 2005; Volume 82.
12. Bohacs, K.M.; Grabowski, G.J.; Carroll, A.R., Jr.; Mankiewicz, P.J.; Miskell-Gerhardt, K.J.; Schwalbach, J.R.; Wegner, M.B.; Simo, J.A. Production, Destruction, and Dilution—The Many Paths to Source-Rock Development. In *The Deposition of Organic-Carbon-Rich Sediments: Models, Mechanisms, and Consequences*; SEPM Society for Sedimentary Geology: Broken Arrow, OK, USA, 2005; Volume 82.
13. Rimmer, S.M.; Thompson, J.A.; Goodnight, S.A.; Robl, T.L. Multiple controls on the preservation of organic matter in Devonian–Mississippian marine black shales: Geochemical and petrographic evidence. *Palaeogeogr. Palaeoclimatol. Palaeoecol.* **2004**, *215*, 125–154. [CrossRef]
14. Wei, C.; Dong, T.; He, Z.; He, S.; He, Q.; Yang, R.; Guo, X.; Hou, Y. Major, trace-elemental and sedimentological characterization of the upper Ordovician Wufeng-lower Silurian Longmaxi formations, Sichuan Basin, south China: Insights into the effect of relative sea-level fluctuations on organic matter accumulation in shales. *Mar. Petrol. Geol.* **2021**, *126*, 104905. [CrossRef]
15. Shen, W.; Wang, Y.; Zheng, Z.; Shen, S.; Xie, H.; Qin, H.; Bai, M. Paleo-Environmental Variation and Its Control on the Organic Matter Accumulation in Black Shale of the Permian Gufeng Formation in the Lower Yangtze Area, South China. *Front. Earth Sci.* **2022**, *10*, 899947. [CrossRef]
16. Canfield, D.E. Factors influencing organic carbon preservation in marine sediments. *Chem. Geol.* **1994**, *114*, 315–329. [CrossRef] [PubMed]
17. Chen, L.; Zhang, B.; Chen, X.; Jiang, S.; Zhang, G.; Lin, W.; Chen, P.; Liu, Z. Depositional environment and organic matter accumulation of the Lower Cambrian Shuijingtuo Formation in the middle Yangtze area, China. *J. Petrol. Sci. Eng.* **2022**, *208*, 109339. [CrossRef]
18. Ibach, L.E.J. Relationship Between Sedimentation Rate and Total Organic Carbon Content in Ancient Marine Sediments1. *AAPG Bull.* **1982**, *66*, 170–188.
19. Liu, Z.; Xu, L.; Wen, Y.; Zhang, Y.; Luo, F.; Duan, K.; Chen, W.; Zhou, X.; Wen, J. Accumulation characteristics and comprehensive evaluation of shale gas in Cambrian Niutitang Formation, Hubei. *Earth Sci.* **2022**, *47*, 1586–1603. (In Chinese)
20. Chen, X.; Chen, L.; Jiang, S.; Liu, A.; Luo, S.; Li, H.; Li, P.; Chen, P. Evaluation of shale reservoir quality by geophysical logging for Shuijingtuo Formation of Lower Cambrian in Yichang area, central Yangtze. *J. Earth Sci.* **2021**, *32*, 766–777. [CrossRef]
21. Wang, Y.; Zhai, G.; Liu, G.; Shi, W.; Lu, Y.; Li, J.; Zhang, Y. Geological characteristics of shale gas in different strata of marine facies in South China. *J. Earth Sci.* **2021**, *32*, 725–741. [CrossRef]
22. Zhang, T.; Luo, H.; Meng, K. Discussion on main controlling factors of the differences of gas content for Cambrian shale in different regions of South China. *Earth Sci. Front.* **2023**, *30*, 1–13. (In Chinese)

23. Wei, S.; Hu, M.; He, S.; Shu, Y.; Dong, T.; He, Q.; Yang, W.; Cai, Q. Effects of Quartz Precipitation on the Abundance and Preservation of Organic Matter Pores in Cambrian Marine Shale in South China. *J. Mar. Sci. Eng.* **2023**, *11*, 1267. [CrossRef]
24. Yang, W.; He, S.; Zhai, G.; Tao, Z.; Yuan, X.; Wei, S. Maturity assessment of the Lower Cambrian and Sinian shales using multiple technical approaches. *J. Earth Sci.* **2021**, *32*, 1262–1277. [CrossRef]
25. Meng, M.; Ge, H.; Shen, Y.; Ji, W.; Li, Z. Insight into water occurrence and pore size distribution by nuclear magnetic resonance in marine shale reservoirs, southern China. *Energy Fuels* **2023**, *37*, 319–327. [CrossRef]
26. Li, Z.X.; Bogdanova, S.V.; Collins, A.S.; Davidson, A.; De Waele, B.; Ernst, R.E.; Fitzsimons, I.C.W.; Fuck, R.A.; Gladkochub, D.P.; Jacobs, J.; et al. Assembly, configuration, and break-up history of Rodinia: A synthesis. *Precambrian Res.* **2008**, *160*, 179–210. [CrossRef]
27. Jiang, G.; Wang, X.; Shi, X.; Xiao, S.; Zhang, S.; Dong, J. The origin of decoupled carbonate and organic carbon isotope signatures in the early Cambrian (ca. 542–520 Ma) Yangtze platform. *Earth Planet. Sci. Lett.* **2012**, *317–318*, 96–110. [CrossRef]
28. Wang, Z.; Tan, J.; Hilton, J.; Dick, J.; Wen, Z. Trace element enrichment mechanisms in black shales during the early cambrian (ca. 521–514 Ma), South China. *Mar. Petrol. Geol.* **2023**, *149*, 106083. [CrossRef]
29. Tribovillard, N.; Algeo, T.J.; Lyons, T.; Riboulleau, A. Trace metals as paleoredox and paleoproductivity proxies: An update. *Chem. Geol.* **2006**, *232*, 12–32. [CrossRef]
30. Taylor, S.R.; McLennan, S.M. The Continental Crust: Its Composition and Evolution. 1985. Available online: https://www.osti.gov/biblio/6582885 (accessed on 17 October 2023).
31. Ross, D.J.K.; Bustin, R.M. Investigating the use of sedimentary geochemical proxies for paleoenvironment interpretation of thermally mature organic-rich strata: Examples from the Devonian–Mississippian shales, Western Canadian Sedimentary Basin. *Chem. Geol.* **2009**, *260*, 1–19. [CrossRef]
32. Abanda, P.A.; Hannigan, R.E. Effect of diagenesis on trace element partitioning in shales. *Chem. Geol.* **2006**, *230*, 42–59. [CrossRef]
33. Raiswell, R.; Berner, R.A. Organic carbon losses during burial and thermal maturation of normal marine shales. *Geology.* **1987**, *15*, 853–856. [CrossRef]
34. Steiner, M.; Wallis, E.; Erdtmann, B.-D.; Zhao, Y.; Yang, R. Submarine-hydrothermal exhalative ore layers in black shales from South China and associated fossils—Insights into a Lower Cambrian facies and bio-evolution. *Palaeogeogr. Palaeoclimatol. Palaeoecol.* **2001**, *169*, 165–191. [CrossRef]
35. Zhang, K.; Li, X.; Wang, Y.; Liu, W.; Yu, Y.; Zhou, L.; Feng, W. Paleo-environments and organic matter enrichment in the shales of the Cambrian Niutitang and Wunitang Formations, south China: Constraints from depositional environments and geochemistry. *Mar. Petrol. Geol.* **2021**, *134*, 105329. [CrossRef]
36. Zhang, K.; Jiang, Z.; Yin, L.; Gao, Z.; Wang, P.; Song, Y.; Jia, C.; Liu, W.; Liu, T.; Xie, X.; et al. Controlling functions of hydrothermal activity to shale gas content-taking lower Cambrian in Xiuwu Basin as an example. *Mar. Petrol. Geol.* **2017**, *85*, 177–193. [CrossRef]
37. Li, Y.; Fan, T.; Zhang, J.; Zhang, J.; Wei, X.; Hu, X.; Zeng, W.; Fu, W. Geochemical changes in the Early Cambrian interval of the Yangtze Platform, South China: Implications for hydrothermal influences and paleocean redox conditions. *J. Asian Earth Sci.* **2015**, *109*, 100–123. [CrossRef]
38. Wang, Z.; Tan, J.; Boyle, R.; Hilton, J.; Ma, Z.; Wang, W.; Lyu, Q.; Kang, X.; Luo, W. Evaluating episodic hydrothermal activity in South China during the early Cambrian: Implications for biotic evolution. *Mar. Petrol. Geol.* **2020**, *117*, 104355. [CrossRef]
39. Boström, K.; Peterson, M.N.A. The origin of aluminum-poor ferromanganoan sediments in areas of high heat flow on the East Pacific Rise. *Mar. Geol.* **1969**, *7*, 427–447. [CrossRef]
40. Yamamoto, K. Geochemical characteristics and depositional environments of cherts and associated rocks in the Franciscan and Shimanto Terranes. *Sediment Geol.* **1987**, *52*, 65–108. [CrossRef]
41. Cai, Q.; Hu, M.; Kane, O.I.; Li, M.; Zhang, B.; Hu, Z.; Deng, Q.; Xing, N. Cyclic variations in paleoenvironment and organic matter accumulation of the Upper Ordovician–Lower Silurian black shale in the Middle Yangtze Region, South China: Implications for tectonic setting, paleoclimate, and sea-level change. *Mar. Petrol. Geol.* **2021**, *136*, 105477. [CrossRef]
42. Dong, T.; He, Q.; He, S.; Zhai, G.; Zhang, Y.; Wei, S.; Wei, C.; Hou, Y.; Guo, X. Quartz types, origins and organic matter-hosted pore systems in the lower cambrian Niutitang Formation, middle yangtze platform, China. *Mar. Petrol. Geol.* **2021**, *123*, 104739. [CrossRef]
43. Adachi, M.; Yamamoto, K.; Sugisaki, R. Hydrothermal chert and associated siliceous rocks from the northern Pacific their geological significance as indication od ocean ridge activity. *Sediment Geol.* **1986**, *47*, 125–148. [CrossRef]
44. Halbach, M.; Halbach, P.; Lüders, V. Sulfide-impregnated and pure silica precipitates of hydrothermal origin from the Central Indian Ocean. *Chem. Geol.* **2002**, *182*, 357–375. [CrossRef]
45. Zhang, Y.; Huang, D.; Zhang, L.; Wan, C.; Luo, H.; Shao, D.; Meng, K.; Yan, J.; Zhang, T. Biogenic silica of the Lower Cambrian Shuijingtuo Formation in Yichang, western Hubei Province—Features and influence on shale gas accumulation. *Earth Sci. Front.* **2023**, *30*, 83–100. (In Chinese)
46. Luo, H.; Shao, D.; Meng, K.; Zhang, Y.; Song, H.; Yan, J.; Zhang, T. Origin of excess barium in the Cambrian shale of Yichang area, western Hubei, and its implication for organic matter accumulation. *Earth Sci. Front.* **2023**, *30*, 66–82. (In Chinese)
47. Wei, K.; Chen, X.; Wang, C.; Liu, A.; Zeng, X.; Li, Z. Origin of siliceous rocks in west Hunan and Hubei Provinces during Late Ediacaran-Early Cambrian, and its geological significance of shale gas. *Bull. Geol. Sci. Technol.* **2020**, *39*, 20–30. (In Chinese)
48. Jones, B.; Manning, D.A.C. Comparison of geochemical indices used for the interpretation of palaeoredox conditions in ancient mudstones. *Chem. Geol.* **1994**, *111*, 111–129. [CrossRef]

49. Gambacorta, G.; Trincianti, E.; Torricelli, S. Anoxia controlled by relative sea-level changes: An example from the Mississippian Barnett Shale Formation. *Palaeogeogr. Palaeoclimatol. Palaeoecol.* **2016**, *459*, 306–320. [CrossRef]
50. Zhao, L.; Liu, S.; Li, G.; Zhang, M.; Liang, X.; Li, J.; Xu, J. Sedimentary Environment and Enrichment of Organic Matter During the Deposition of Qiongzhusi Formation in the Upslope Areas—A Case Study of W207 Well in the Weiyuan Area, Sichuan Basin, China. *Front. Earth Sci.* **2022**, *10*, 867616. [CrossRef]
51. Hoefs, J. *Stable Isotope Geochemistry*; Springer: Berlin/Heidelberg, Germany, 1997; Volume 201.
52. Algeo, T.J.; Ingall, E. Sedimentary Corg:P ratios, paleocean ventilation, and Phanerozoic atmospheric pO2. *Palaeogeogr. Palaeoclimatol. Palaeoecol.* **2007**, *256*, 130–155. [CrossRef]
53. Ingall, E.; Kolowith, L.; Lyons, T.; Hurtgen, M. Sediment carbon, nitrogen and phosphorus cycling in an anoxic fjord, Effingham Inlet, British Columbia. *Am. J. Sci.* **2005**, *305*, 240–258. [CrossRef]
54. Sannigrahi, P.; Ingall, E. Polyphosphates as a source of enhanced P fluxes in marine sediments overlain by anoxic waters: Evidence from 31P NMR. *Geochem. Trans.* **2005**, *6*, 52–59. [CrossRef]
55. Luo, S.; Chen, X.; Li, H.; Wang, C. Shale gas accumulation conditions and target optimization of the Lower Cambrian Shuijintuo Formation in Yichang area, Western Hubei. *Earth Sci.* **2019**, *44*, 3598–3615. (In Chinese)
56. Algeo, T.J.; Tribovillard, N. Environmental analysis of paleoceanographic systems based on molybdenum–uranium covariation. *Chem. Geol.* **2009**, *268*, 211–225. [CrossRef]
57. Tribovillard, N.; Algeo, T.J.; Baudin, F.; Riboulleau, A. Analysis of marine environmental conditions based onmolybdenum–uranium covariation—Applications to Mesozoic paleoceanography. *Chem. Geol.* **2012**, *324–325*, 46–58. [CrossRef]
58. Zhang, G.; Chen, D.; Ding, Y.; Huang, T. Controls on Organic Matter Accumulation from an Upper Slope Section on the Early Cambrian Yangtze Platform, South China. *Minerals* **2023**, *13*, 260. (In Chinese) [CrossRef]
59. Yang, X.; Yan, D.; Zhang, B.; Zhang, L.; Wei, X.; Li, T.; Zhang, J.; She, X. The impact of volcanic activity on the deposition of organic-rich shales: Evidence from carbon isotope and geochemical compositions. *Mar. Petrol. Geol.* **2021**, *128*, 105010. [CrossRef]
60. Shu, Y.; Lu, Y.; Hu, Q.; Wang, C.; Wang, Q. Geochemical, petrographic and reservoir characteristics of the transgressive systems tract of lower Silurian black shale in Jiaoshiba area, southwest China. *Mar. Petrol. Geol.* **2021**, *129*, 105014. [CrossRef]
61. Shen, W.; Zhu, X.; Li, J.; Yan, B. Mechanism of organic matter accumulation in black shale of the Datangpo Formation: Insights from paleo-environmental variation during the Cryogenian non-glaciation. *Precambrian Res.* **2022**, *383*, 106889. [CrossRef]
62. Rimmer, S.M. Geochemical paleoredox indicators in Devonian–Mississippian black shales, Central Appalachian Basin (USA). *Chem. Geol.* **2004**, *206*, 373–391. [CrossRef]
63. Thibault, N.; Ruhl, M.; Ullmann, C.V.; Korte, C.; Kemp, D.B.; Gröcke, D.R.; Hesselbo, S.P. The wider context of the Lower Jurassic Toarcian oceanic anoxic event in Yorkshire coastal outcrops, UK. *Proc. Geol. Assoc.* **2018**, *129*, 372–391. [CrossRef]
64. Yi, F.; Yi, H.; Xia, G.; Wu, C.; Li, G.; Cai, Z.; Li, N. Factors controlling the organic matter accumulation across the Pliensbachian-Toarcian transition in the Qiangtang Basin, Tibetan Plateau. *Mar. Petrol. Geol.* **2021**, *133*, 105304. [CrossRef]
65. Dong, T.; Harris, N.B.; Knapp, L.J.; McMillan, J.M.; Bish, D.L. The effect of thermal maturity on geomechanical properties in shale reservoirs: An example from the Upper Devonian Duvernay Formation, Western Canada Sedimentary Basin. *Mar. Petrol. Geol.* **2018**, *97*, 137–153. [CrossRef]
66. Cai, Q.; Hu, M.; Kane, O.I.; Yang, Z.; Wen, Y.; Luo, Q.; Li, M.; Hu, Z.; Deng, Q. Petrological and geochemical characteristics of the Ordovician–Silurian black shale in eastern Sichuan and western Hubei, South China: Differential sedimentary responses to tectonism and glaciation. *J. Palaeogeogr.* **2023**, *12*, 129–152. [CrossRef]
67. Worden, R.H.; Morad, S. Quartz cementation in oil field sandstones: A review of the key controversies. In *Quartz Cementation in Sandstones*; Worden, R.H., Morad, S., Eds.; Blackwell Science: Hoboken, NJ, USA, 2000; pp. 1–20.
68. Rutman, P.; Hoareau, G.; Kluska, J.-M.; Lejay, A.; Fialips, C.; Gelin, F.; Aubourg, C.; Bilbao, E.H. Diagenesis and alteration of subsurface volcanic ash beds of the Vaca Muerta Formation, Argentina. *Mar. Petrol. Geol.* **2021**, *132*, 105220. [CrossRef]
69. Dong, T.; Harris, N.B.; Ayranci, K.; Yang, S. The impact of rock composition on geomechanical properties of a shale formation: Middle and Upper Devonian Horn River Group shale, Northeast British Columbia, Canada. *AAPG Bull.* **2017**, *101*, 177–204. [CrossRef]
70. Zhao, J.; Jin, Z.; Lin, C.; Liu, G.; Liu, K.; Liu, Z.; Zhang, Y. Sedimentary environment of the Lower Cambrian Qiongzhusi Formation shale in the Upper Yangtze region. *Oil Gas Geol.* **2019**, *40*, 701–715. (In Chinese)

Disclaimer/Publisher's Note: The statements, opinions and data contained in all publications are solely those of the individual author(s) and contributor(s) and not of MDPI and/or the editor(s). MDPI and/or the editor(s) disclaim responsibility for any injury to people or property resulting from any ideas, methods, instructions or products referred to in the content.